J Intell Robot Syst (2011) 63:399–416
DOI 10.1007/s10846-010-9516-6

A Novel Swimming Microrobot Based on Artificial Cilia for Biomedical Applications

Ali Ghanbari · Mohsen Bahrami

Received: 6 June 2010 / Accepted: 7 December 2010 / Published online: 22 March 2011

Abstract Swimming microrobots can exhibit high levels of performance to move freely in the human body fluids to fulfill risky biomedical operations by mimicking microorganisms. Many researchers have proposed micro swimming methods for viscous flows based on flagellar motion. Here, a novel swimming microrobot inspired by ciliated microorganisms based on artificial cilia is introduced. The hydrodynamic model is developed and performance parameters such as propulsive force, propulsive velocity and efficiency of the microrobot are computed. The velocity and efficiency dependence on design parameters of microrobot is evaluated. The proposed micro swimming concept offers appropriate efficiency, thrust, speed and maneuverability. It is shown that the introduced swimming microrobot can reach a maximum speed 4.5 mm/s and efficiency of 40%. The proposed microrobot has the potential to be utilized in both viscous and turbulent body flows.

Keywords Swimming microrobots · Ciliary motion · Artificial cilia · Efficiency · Biomedical microrobots

1 Introduction

Microelectromechanical systems (MEMS) and nanoelectromechanical systems (NEMS) technology have brought new promises for treatment of diseases in a

A. Ghanbari · M. Bahrami (✉)
Mechanical Engineering Department,
Amirkabir University of Technology, Tehran, Iran
e-mail: mbahrami@aut.ac.ir

A. Ghanbari
e-mail: aghanbari@aut.ac.ir

more accurate way and with fewer side effects. Tiny MEMS/NEMS components and devices, created by micromachining technology, can be integrated into a microrobot and entered into the human body with minimum interferences. Miniaturization of robots makes them particularly useful for medical applications, such as precise drug delivery to diseased or defected organs inside the human body or minimally invasive surgery [1]. For such operations, a microrobot should have the characteristic dimensions of few tenths of one millimeter. Swimming microrobots can play a key role in medical applications for in vivo drug delivery, monitoring early symptoms of diseases and minimally invasive surgery.

In nature, microorganisms use different techniques for swimming: eukaryotic flagellar motion, prokaryotic flagellar motion and ciliary motion. Eukaryotic and prokaryotic flagellar motion implies cells propulsion by bending and rotating the flagella protruding from the cell body, respectively. Cilia are shorter organelles versus flagella but larger in quantity.

In this paper, we introduce a novel methodology for swimming at low Re numbers inspired by *Paramecium* based on ciliary motion. In contrast to the variety of flagella-based swimming microrobots, an artificial microswimmer based on ciliary propulsion has not yet been realized. The proposed microrobot, which we call it *ParaLiker*, swims using artificial cilia. We model the microrobot dynamics and solve the coupled elastic-fluidic nonlinear system to prove the concept. Designing the microrobot, the effect of different parameters on its motion is analyzed. We compute the efficiency of the proposed microswimmer and show how it changes with independent design parameters. The performance of the swimming methodology is determined with considering two different engines for cilia actuation, one similar to the natural cilia internal engine and one simple engine.

ParaLiker has two arrays of cilia with in-plane beating action that generates thrust against fluid resistive force, which pushes the microrobot forward. Solving the microrobot dynamics, it is shown that the swimming methodology based on artificial cilia generates a reasonable thrust possessing a relatively high efficiency for drag-based swimming. The cilia for the suggested swimming microrobot act like paddles for a boat and although the microrobot is supposed to work in low Re environments, however it can also be used in turbulent flows in human body.

2 Related Work

There are fish-like swimming microrobots introduced in the literature [2–5]. The methodologies used for propulsion of fish-like microrobots are based on inertial forces. Large Reynolds (Re) number theory models the motion of these microrobots for which propulsive mechanisms rely clearly on the reaction of the fluid to acceleration. Although the size of proposed fish-like robots is often too large to enter into the human body, but the main challenge is the propulsion methodology. Even though the inefficiency of inertia-based swimming for low Re numbers is already known, Uchiyama and Kikuyama [6] properly demonstrated this point. Analyzing a wiggling micromachine propulsive performance, they showed that the thrust force reduces with decrement of Re, when Re is between 10 and 100. For $\mathrm{Re} < 10$ this decrement is remarkable and propulsive force is completely lost for Re less than one.

Several swimming microrobots have been developed inspired by nature [7–17]. Behkam and Sitti [7] introduced two methodologies based on flagellar motion for propulsion of swimming microrobots and developed the related hydrodynamic models. Since power is limited at microscale, the efficiency of microrobot is a critical performance parameter. The efficiency of microrobots developed by Behkam and Sitti is fairly low [7]. Based on eukaryotic flagellation, another swimming microrobot proposed by Kosa et al. uses travelling waves in elastic tails for propulsion [8]. Voltages of same frequency and different phases stimulate the tails, which are composed of piezoelectric segments. Therefore, a travelling wave is created through the tail. In another design introduced by Li et al. [9], a spiral-type head is connected to an elastic tail to form a swimming microrobot. By applying an external magnetic field, the head rotates and the helical wave formed in the elastic tail produces the propulsion force for the microrobot. Yesin et al. applied an external magnetic field to pull a magnetized submillimeter-sized device [10]. Guo et al. [11] and Zhang et al. [12] devised two swimming propulsion systems based on planar and helical wave formed in the artificial flagella attached to the body of microrobot, respectively. The performance of these three devices, which all are driven magnetically, has been investigated and compared in a work by Abbott et al. [13]. They concluded that the helical flagellar propulsion outperforms the magnetic gradient pulling and is likely the best solution.

Some researchers have shown interest in the utilization of biological elements or microorganisms as propulsion system for artificial microswimmers. For instance, Dreyfus et al. [18] used a chain of magnetic spheres attached by DNA linkers to transport a blood cell. Beating in the chain is produced by applying two magnetic fields in different directions. In another study, a flagellated Magnetotactic Bacterium (MTB) was used as propulsion system for a nanorobot operating in human body vessels [19]. The nanorobot was controlled and tracked through microfluidic channels using a Magnetic Resonance Imaging (MRI) system. A work by Behkam and Sitti [20] also fits in this branch of research for microswimming propulsion. They utilized a cell of bacteria for propulsion of a swimming body.

Recently, many researchers have developed artificial cilia [21–24]. Artificial cilia advantages make them reasonable for a wide variety of applications. They can be batch-fabricated and used as sensors and actuators.

As per nature of swimming by flagella, low efficiency is expected [25]. The proposed microrobots in literature have a low efficiency and it seems that a more efficient methodology is required for swimming at microscale. Here, we propose a swimming methodology inspired by ciliary motion of microorganisms. We show that the proposed microrobot has a reasonable thrust, velocity and efficiency. The study presented here can be used as a methodology for an artificial microswimmer with a desired motion. The most intriguing application of this microswimmer can be for biomedical tasks inside the human body.

3 Concept

Methods and physics of swimming at microscale are different to that at macroscale. In microsystems, inertial forces play little role and viscous forces are dominant. The immediate consequence of dominance of viscous forces in a fluid flow over inertial

forces is a low Re number. Hydrodynamics of a fluid flow is governed by Navier–Stokes equations:

$$\rho\left(\frac{\partial \mathbf{u}}{\partial t} + \mathbf{u}.\nabla\mathbf{u}\right) = \rho\mathbf{g} + \mu\nabla^2\mathbf{u} - \nabla p, \qquad \nabla.\mathbf{u} = 0 \tag{1}$$

where ρ and μ are the density and dynamic viscosity of fluid, $\mathbf{u}$ is the fluid velocity, $\mathbf{g}$ is the gravitational acceleration and p is the pressure. For viscous flows, it is appropriate to study the limiting case of Re $= 0$, for which the inertial terms disappear in Eq. 1 and it simplifies to Stokes equation

$$\nabla p = \mu\nabla^2\mathbf{u}, \qquad \nabla.\,\mathbf{u} = 0 \tag{2}$$

Microorganisms use cilia and flagella to generate a propulsive force in fluids. Cilia (with a typical length of 10–15 μm) are hair-like appendages of microorganisms like *Paramecium* (Fig. 1). Cilia beat in a cyclic pattern and force microorganism to move forward. Since time is not present in Eq. 2, if the two parts of cilia motion are the same, there would not be any net displacement for microorganism. Therefore, the beating cycle of cilia has two different parts: power stroke, which in cilia are straight and beat on the fluid to thrust the microorganism, and recovery stroke, which cilia bow to have minimal effect on the fluid.

ParaLiker inspired by *Paramecium*, depicted schematically in Fig. 2, uses artificial cilia to generate required propulsion. It has two arrays of artificial cilia beating synchronously and a body, which can encompass various microrobot parts such as control unit, components for remote control, camera, actuation system, drug delivery

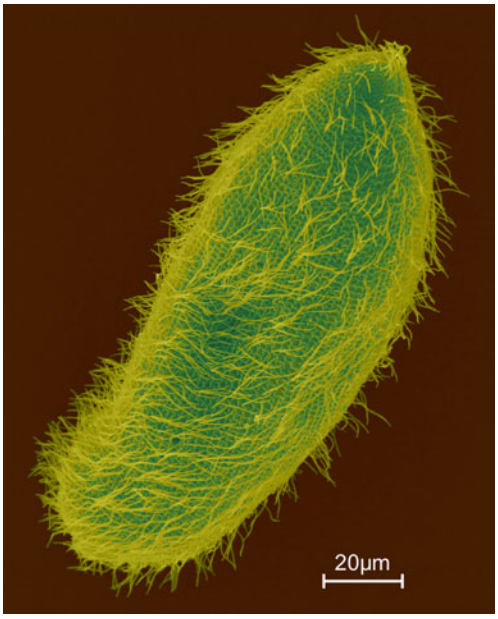

Fig. 1 *Paramecium* SEM image Copyright Dennis Kunkel Microscopy, Inc

Fig. 2 Schematic of *ParaLiker*

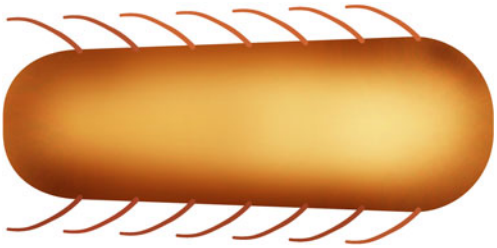

unit, etc. The microrobot can move forward by artificial cilia beating backward in a straight form, and returning them in a bent shape. Conversely the microrobot can move backward by beating the cilia to the forth. Here, to demonstrate the applicability of the concept, we study the planner motion of *ParaLiker*.

4 Microrobot Design

Microrobot body is an ellipsoid, which closely mimics the *Paramecium* natural shape. Cilia are considered as cylindrical filaments of length L and diameter d. The number of cilia is assumed to be N. In this section, we provide the required knowledge to design the proposed microrobot, along with some motion modeling and analysis.

4.1 Hydrodynamics of Cilia

The first step to prove the feasibility of a propulsion system is to develop a dynamic model. For this purpose, the hydrodynamics of cilia should be explored. Research for modeling the interactions of flagella and cilia with fluid has been initiated many years ago [26]. We can categorize mathematical modeling of ciliary motion in two major theories: resistive force theory (RFT) and slender body theory (SBT). RFT relates drag forces exerted on cilia by fluid in tangential, normal and binormal directions to the local velocity in the same directions. Gray and Hancock established RFT concept [27], on which many later works were based. The constant of proportionality of drag force to local velocity (resistance coefficient) has been the place of debate and can be found in literature with different values [27–30].

The schematic of a cilium along with the global and local systems of coordinates are shown in Fig. 3. Drag force in tangential and normal direction can be obtained from approximation developed by [27]

$$\phi_T(s,t) = -C_T V_T(s,t) \tag{3}$$

$$\phi_N(s,t) = -C_N V_N(s,t) \tag{4}$$

where T and N denotes tangential and normal directions. V_T, V_N, C_T, C_N, ϕ_T and ϕ_N are tangential and normal velocities, resistance coefficients and drag forces, respectively. Noting that cilia are slender, the resistance coefficients are [29]

$$C_T = \frac{8\pi\mu}{-2 + 4\ln\left(4q/d\right)} \tag{5}$$

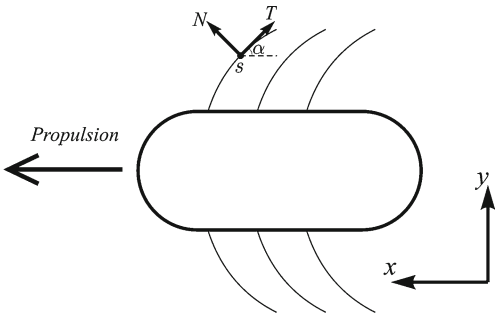

Fig. 3 Local and global coordinate systems

$$C_N = \frac{8\pi\mu}{1 + 2\ln\left(4q/d\right)} \tag{6}$$

where d is the cilium diameter and q is an arbitrary value provided that $q/L << 1$, $d/q << 1$, where L is the cilium length.

Cilium is modeled as an inextensible filament. The tangent to the centerline of cilium, shown in Fig. 3 at point s (arc length parameter along centerline of cilium) and time t, makes an angle of $\alpha(s,t)$ with x axis. Velocities in tangential and normal directions are related thorough geometrical equations [31]

$$\frac{\partial V_N}{\partial s} = \frac{\partial \alpha}{\partial t} - V_T \frac{\partial \alpha}{\partial s} \tag{7}$$

$$\frac{\partial V_T}{\partial s} = V_N \frac{\partial \alpha}{\partial s} \tag{8}$$

which are geometrical constraints for ciliary motion. Force and moment balance yield

$$\frac{\partial F_T}{\partial s} - F_N \frac{\partial \alpha}{\partial s} = \phi_T \tag{9}$$

$$\frac{\partial F_N}{\partial s} + F_T \frac{\partial \alpha}{\partial s} = \phi_N \tag{10}$$

$$\frac{\partial M}{\partial s} = F_N \tag{11}$$

where F and M denotes internal force and moment of cilium.

Artificial cilia should be actuated for microrobot propulsion. Regardless of actuation method, the internal moment of cilia is composed of two parts. First part is due to the actuation force. Second part arises from beam elasticity. If cilium is considered as a beam, the beam bending moment is obtained from $M = EI\kappa$, where $\kappa = \frac{\partial \alpha}{\partial s}$, E is the Young modulus of cilium material and I is the second moment of area of cilium cross section. EI is called flexural stiffness. From Eq. 11, we have

$$F_N = EI \frac{\partial^2 \alpha}{\partial s^2} + A \tag{12}$$

where $A(s,t)$ is the applied actuation force which is shown in a modular manner.

Equations 7–12 are solved simultaneously to find the drag forces exerted on cilia and other unknowns, such as shape of cilia (α), velocity of cilia, internal forces and moment of cilia. Differentiating Eqs. 9 and 10 and using Eqs. 5–8 and again using Eqs. 9 and 10, two equations which relate F_T, F_N and α are derived as

$$\frac{\partial^2 F_T}{\partial s^2} = \left(1 + \frac{C_T}{C_N}\right) \frac{\partial F_N}{\partial s} \frac{\partial \alpha}{\partial s} + \frac{C_T}{C_N} F_T \left(\frac{\partial \alpha}{\partial s}\right)^2 + F_N \frac{\partial^2 \alpha}{\partial s^2} \tag{13}$$

$$\frac{\partial^2 F_N}{\partial s^2} + \left(1 + \frac{C_N}{C_T}\right) \frac{\partial F_T}{\partial s} \frac{\partial \alpha}{\partial s} + F_T \frac{\partial^2 \alpha}{\partial s^2} + C_N \frac{\partial \alpha}{\partial t} = \frac{C_N}{C_T} F_N \left(\frac{\partial \alpha}{\partial s}\right)^2 \tag{14}$$

Equations 12–14 form three partial differential equations with nonlinear terms and should be solved numerically to find F_T, F_N and α for total time span, from beginning of power stroke to the end of cilia beating and for all points along cilia (for details see [32]).

4.2 Equations of Motion

We develop a dynamic model of the *ParaLiker* system that takes the dimensions and hydrodynamics of cilia as input and returns performance parameters, such as propulsion force and velocity. Neglecting inertial forces, force balance is written as

$$\sum \mathrm{F}_{x,\,\mathrm{cilia}} + \sum \mathrm{F}_{x,\,\mathrm{body}} = 0 \tag{15}$$

$$\sum \mathrm{F}_{y,\,\mathrm{cilia}} + \sum \mathrm{F}_{y,\,\mathrm{body}} = 0 \tag{16}$$

and moment balance in out of plane direction:

$$\sum \mathrm{M}_{\mathrm{cilia}} + \sum \mathrm{M}_{\mathrm{body}} = 0 \tag{17}$$

For an element ds on one cilium, forces in x and y directions during power stroke of cilium is

$$dF_{x,\,\mathrm{cilium}} = -\phi_T ds \cos\alpha + \phi_N ds \sin\alpha \tag{18}$$

$$dF_{y,\,\mathrm{cilium}} = \phi_N ds \cos\alpha + \phi_T ds \sin\alpha \tag{19}$$

where ϕ_T and ϕ_N are tangential and normal drag forces and can be obtained from

$$\phi_T = -C_T (V_T - U\cos\alpha) \tag{20}$$

$$\phi_N = -C_N (V_N + U\sin\alpha) \tag{21}$$

where U is the velocity of microrobot body.

We consider arrays of cilia symmetrically about the centerline of microrobot body (on both sides for planar motion). $F_{y,\mathrm{cilia}}$ is the same for the cilia on both sides of

the microrobot but in opposite direction, eliminating each other in Eq. 16. This also applies to the resultant moments due to $F_{x,\text{cilia}}$ about centerline of body. Since, there is no other force in y direction and no moment acting on the body of the microrobot, Eqs. 16 and 17 are satisfied. Substituting Eqs. 20 and 21 into Eq. 18:

$$dF_{x,\,\text{cilium}} = \left(C_T V_T \cos\alpha - C_T U \cos^2\alpha - C_N V_N \sin\alpha - C_N U \sin^2\alpha\right) ds \tag{22}$$

Integrating Eq. 22, the total force of cilia in x direction is determined from

$$F_{x,\,\text{cilia}} = N \int dF_{x,\,\text{cilium}} \tag{23}$$

where N is the number of cilia attached to the body.

For slow moving bodies through a fluid where Re is low, drag force is proportional to velocity of the body. If microrobot body is considered as an ellipsoid, the drag force ($F_{x,\text{body}}$) in the direction parallel to longitudinal centerline of the ellipsoid is obtained from [33]

$$F_{x,\,\text{body}} = 8.5\mu r U \tag{24}$$

where r is the ellipsoid minor radius. Equations 15 and 22–24 are used to compute forward propulsive velocity of microrobot. $F_{x,\text{cilia}}$ is the propulsive force acting on the microrobot.

4.3 Numerical Example

To have a general view of function of a swimming microrobot based on artificial cilia, a microrobot is designed and the main performance parameters are calculated. Artificial cilia can be fabricated using various methods from different materials. However, the artificial cilia should expose necessary flexibility for sufficient bending through the recovery stroke. As a first estimate, the modulus of elasticity of natural cilia is set in the numerical calculations for E (5 GPa) [34].

Microrobot body size is subject to the size of necessary components for performing in vivo operations. As an assumption in this study, microrobot swims in water. Main design parameters used in numerical example are listed in Table 1.

Term A in Eq. 12 is the actuation force generated in cilia. A is considered as an engine like the one used in [32] to generate a beating pattern similar to what we

Table 1 Microrobot design parameters

Design parameter	Value
Cilium length, L_{cilia}	15 μm
Cilium diameter, d_{cilia}	25 nm
Cilium Young's modulus, E	5 GPa
Body radius, r_{body}	150 μm
Body length, L_{body}	400 μm
Number of cilia, N	40
Water viscosity, μ_{water}	0.001 kg/(ms)

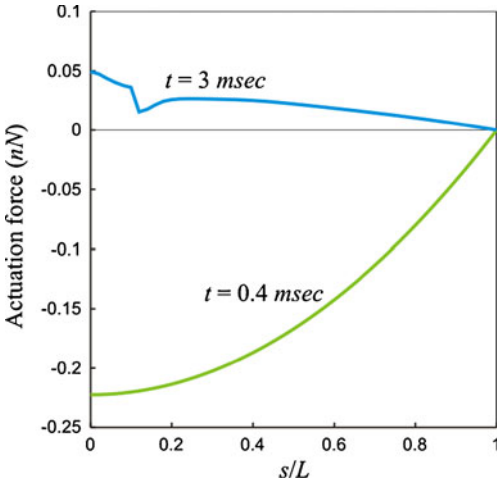

Fig. 4 Actuation force applied on one cilium at t = 0.4 ms (power stroke) and t = 3 ms (recovery stroke) as a function of nondimensional length

see in microorganisms such as *Paramecium*. This engine generates a force, which results in two different patterns for power and recovery strokes of cilia. This force has been plotted at two positions of cilia in Fig. 4, one in power stroke and the other in recovery stroke period.

A computer program has been written to numerically solve the cilia hydrodynamics and microrobot dynamics. Cilium is divided into 50 elements and time step for numerical solution is $dt = 0.1$ msec. Starting with Eq. 12 which takes the initial angle of cilium $\alpha(s, 0)$ and $A(s, 0)$, F_N is determined. Knowing α and F_N, Eq. 13 is an ordinary differential equation for F_T and can be solved numerically. Finally, Eq. 14 which is a nonlinear PDE for α with a fourth-order derivative with respect to s is solved using a finite difference method to propagate α during time. Cilium beating is shown in Fig. 5.

Knowing cilia hydrodynamics and dimensions, dynamic model computes the performance parameters. Figure 6 displays the propulsive force and velocity during a beating cycle of cilia. Power stroke commences from $\alpha = 160°$ and continues to about $\alpha = 20°$, when propulsive force and consequently velocity of microrobot increases from start to a peak point where is at $\alpha = 90°$ and then decreases. This behavior is acceptable since the reaction of force exerted by cilia on fluid is completely in x

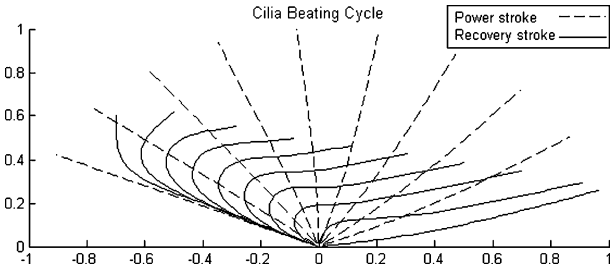

Fig. 5 Schematic of cilia beating due to the actuation with a force shown in Fig. 4

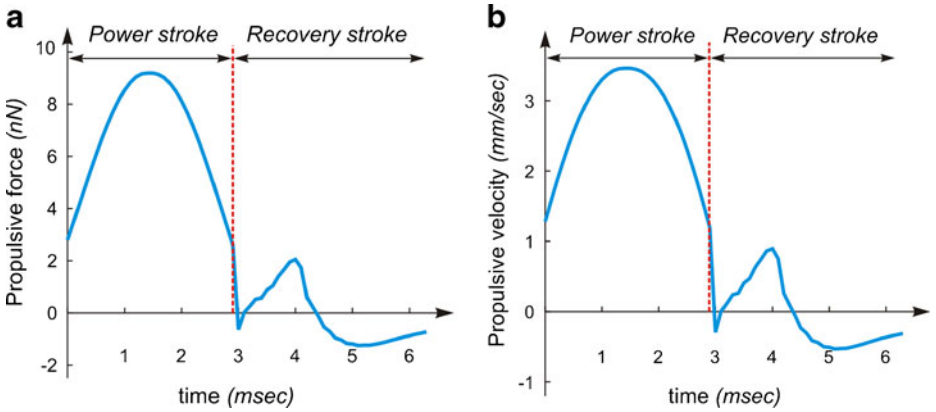

Fig. 6 **a** Propulsive force **b** propulsive velocity of the microrobot for one beating cycle of cilia as a function of time

direction, just when cilia are erect and in other angles of cilia, it only has a component in the direction of robot propulsion. As seen in Fig. 6, the propulsive velocity for recovery stroke is much less than that of power stroke, which makes microrobot enable to have net forward movement.

Figure 7 shows how velocity changes with cilia diameter and length. Except for the values shown, the other parameters are the same as Table 1. An increase in both diameter and length of cilia yield an increase in the velocity of microrobot. However, velocity is more sensitive to the length of cilia. Increasing the diameter of cilia is constrained by flexural stiffness and slenderness property, which should be satisfied. As cilia become thicker, the flexural stiffness will increase which restricts the bending during recovery stroke. Cilia should be thin enough to bend easily to have minimal

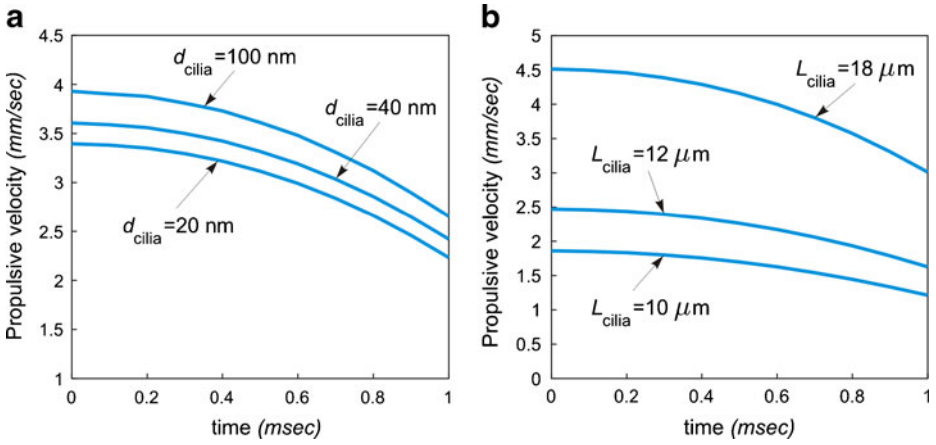

Fig. 7 Velocity of the microrobot during power stroke for different **a** diameters **b** lengths of cilia for 1 msec run after $\alpha = 90°$

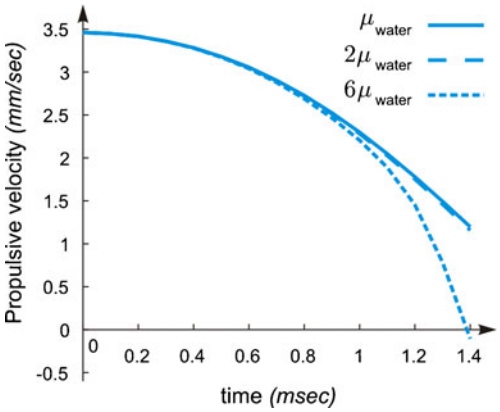

Fig. 8 Velocity of the microrobot in fluid with viscosity of μ_{water}, 2 μ_{water} and 6 μ_{water} during power stroke for 1.4 msec run after $\alpha = 90°$

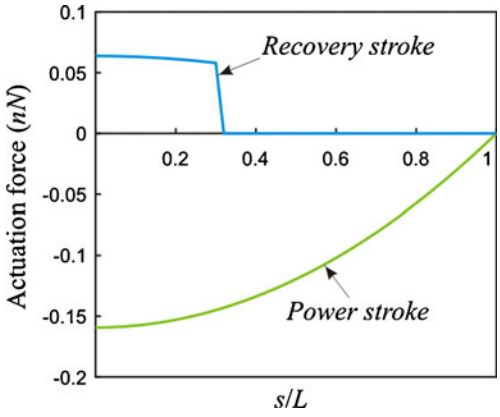

Fig. 9 An actuation force which leads to a fairly symmetric cilia beating

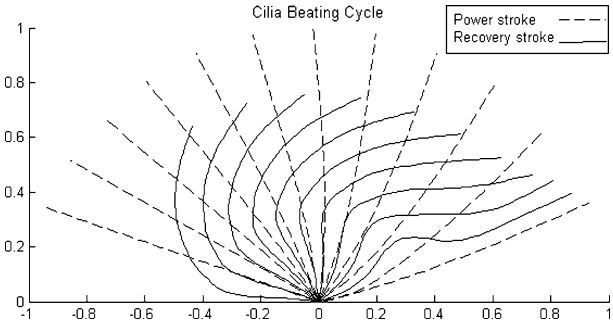

Fig. 10 Shape of cilia during a fairly symmetric beating

effect on the fluid during recovery stroke. Drag forces on cilia increase with the increment of cilia length. Increase in drag forces produce more propulsive force and cause an increase in velocity of the robot, not with a linear proportionality rather with a rapid rise. The interactions between neighboring cilia should be considered as a constraint for making cilia longer.

Figure 8 displays how viscosity of surrounding fluid affects robot velocity. Viscosity has both positive and negative effects on propulsion of the microrobot. As viscosity of the fluid increases, at early stages, there is a balance between these propulsive and preventive effects. However, the velocity of the robot suddenly drops after a few tenths of millisecond. Actually, the microrobot needs more actuation force to move forward.

Our study indicates that the Young modulus of cilia does not cause a significant change in performance of microrobot but makes cilia more rigid, which should be taken into consideration.

The actuation force shown in Fig. 4 for recovery stroke might be hard to be generated. We have considered here a simple actuation force as

$$A(s,t) = C\left(\left(\frac{s}{L}\right)^2 - 1\right) \tag{25}$$

where C is a constant and is taken to be $C = 0.159$ nN and $C = -0.0637$ nN for power and recovery stroke, respectively. As seen in Fig. 9, this actuation force remains unchanged for different times during a power or recovery stroke and in latter case, actuation force is near constant for first three-tenths of cilium length and becomes zero for the rest. This driving actuation force makes cilia start beating as in Fig. 10. Microrobot swims with the velocity depicted in Fig. 11 with a magnitude for recovery stroke, which is comparable to but yet less than one for power stroke. Hence, the robot can move forward.

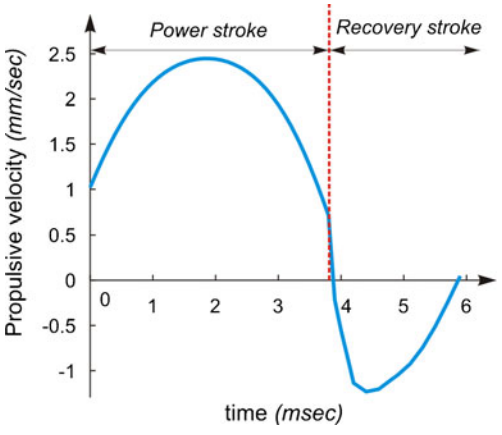

Fig. 11 Velocity of microrobot computed in the case of a fairly symmetric cilia beating

5 *ParaLiker* Efficiency

One of the key parameters that show the performance of a swimming microrobot is hydrodynamic efficiency. Efficiency depends on the methodology of swimming or to critical design parameters of the method. Our calculations for the efficiency reflect that how efficient the swimming by artificial cilia is and what parameters affect the efficiency of ciliary propulsion for microrobot.

ParaLiker has two operational stages: (1) Effective propulsion: cilia consume energy and microrobot moves forward. (2) Cilia reversion: cilia use energy to recover their shape and position to the beginning of power stroke, but the generated energy causes backward propulsion and is undesired. Hydrodynamic efficiency can be obtained from the ratio of energy generated for propulsion of microrobot (with positive sign for effective direction and negative sign for reverse direction) to the energy spent by cilia. Efficiency is calculated for a thorough beating cycle. Gueron and Levit–Gurevich [35] wrote relationships for computing the energy consumption of a cilium. Input energy (E_{in}), the energy spent by N cilia for a beating cycle can be obtained from

$$E_{\text{in}} = N \int_{\text{Beating cycle}} \left(\int_0^{L_{\text{cilia}}} (\phi_T V_T + \phi_N V_N)\, ds \right) dt \tag{26}$$

The energy of propulsion is calculated as

$$E_{\text{out}} = \int_{\text{Power stroke}} \left(F_{x,\,\text{cilia}} U\right) dt - \int_{\text{Return stroke}} \left(F_{x,\,\text{cilia}} U\right) dt \tag{27}$$

Efficiency, defined as $\eta = E_{\text{out}} / E_{\text{in}}$, is computed and shown in Fig. 12, for the robot with design parameters of Table 1, as a function of cilia diameter, cilia length, number of cilia, and radius of microrobot body.

One can observe from Fig. 12 that:

1. Cilia length and diameter have an optimum point for the efficiency of microrobot, that is efficiency first rises up to a pick value and then falls with increasing the cilia dimensions.
2. Number of cilia drastically affects the efficiency of the microrobot. However, beyond a certain value of cilia number, increasing the number of cilia has no longer a noticeable effect on efficiency.
3. The decrement of the microrobot body size elicits a considerable advance in the efficiency; however, it might restrict the ability to carry the required payload.

As shown in Fig. 11, the microrobot with actuation force of Eq. 25 has a net movement. The efficiency of the robot in this condition is 5.9%. It should be noted that this value of efficiency is for a microrobot with 40 cilia. Since the efficiency is dependent on the number of cilia, it can be increased by increasing the number of cilia.

6 Discussion

Performance parameters computed for the microrobot shows that *ParaLiker* has considerable potentials for biomedical in vivo applications. Although, the proposed

idea of using artificial cilia for propulsion of robots at the microscale has its own challenges, however the benefits of ciliary micro swimming are strong motivations for further related studies. Some issues and advantages of micro swimming based on artificial cilia are discussed in the following.

6.1 Cilia Microfabrication

Wide applications of cilia such as micro-fluidic mixing, fluid accelerating and sensing have attracted researchers to fabricate artificial cilia, which mimic natural cilia [22–24, 36]. Magnetic nanowires including permanently magnetic thin films, magnetized polymers and magnetized structures of smart materials form a main type of artificial cilia [21]. Magnetic actuation is the most powerful way of wireless and remote actuation. To generate motion with a controlled shape for cilia, two magnetic fields may be applied. A field provokes straight beating of cilia. In addition, a time-varying field creates a bent configuration to the cilia during recovery stroke.

Another approach for fabrication of artificial cilia is the piezoelectric material utilization. Kosa et al. used a three segment piezoelectric layered beam to construct an artificial flagellum [8]. The same idea can be applied for artificial cilia. A cilium made of several piezoelectric segments, which are stimulated separately with

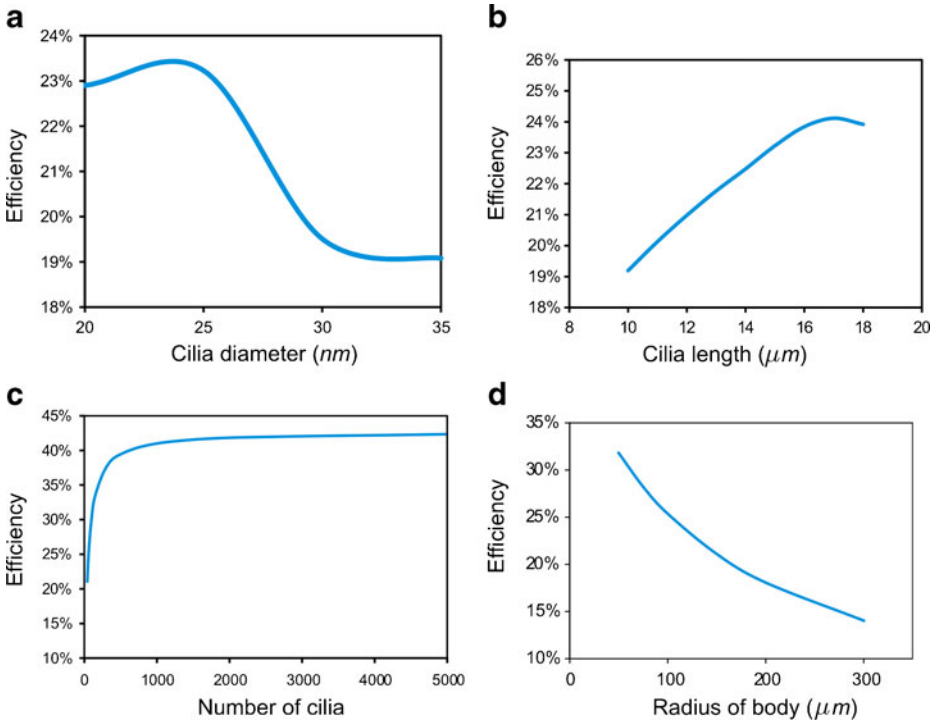

Fig. 12 Efficiency of microrobot as a function of **a** cilia diameter, **b** cilia length, **c** number of cilia, **d** radius of microrobot body

different phases and amplitudes can beat erectly during power stroke and bend in recovery stroke.

Chemically excited material is the third possibility, which makes artificial cilia feasible. Tabata et al. developed a chemo-mechanical actuator to mimic cilia motion [37]. Cilia of the human body convert energy of hydrolysis of chemicals to the mechanical work and chemically excited structures can be utilized as a biocompatible material for artificial cilia. Slow motion is the drawback of these materials.

Biological components might be utilized to act as artificial cilia. The method can be similar to the one used by Dreyfus et al. for fabrication of flagella [18]. The cilia fabricated with this methodology are biocompatible. They can be controlled using chemical or physical mechanisms of the human body.

6.2 Control and Maneuverability

In this paper, the *ParaLiker* was assumed to have one degree of freedom and swims forward and backward along its body centerline. However, the methodology of ciliary swimming has potential for propulsion in higher degrees of freedom. We have arrays of cilia attached to the body of microrobot. Choosing when and which cilia beat can change the orientation of swimming. To float freely in fluid with a high maneuverability, a microswimmer should be controllable. Frequency of beating, duration of power stroke and turning cilia beatings on and off can be used for controlling the robot.

Control of a large number of artificial cilia is a challenge facing the cilia based micro swimming methodology. The aforementioned piezoelectric actuation of cilia is more complicated to be controlled and needs more hardware. Using smart material with no requirement to microchips makes the control convenient.

6.3 Performance

For animals, locomotory efficiency and maximum speed provide relative criteria of functional superiority [38]. At moderate and high Re numbers, larger animals generally swim faster than smaller ones do [39]. For low Re swimmers, we see the same paradigm but a little different. Flagellates speed remains constant with increasing the body length. In contrast, bigger ciliates swim faster. The speed increases directly with body length, in fact, with the number of cilia covering the body. On the other hand, the efficiency of ciliary propulsion does seem to be more than flagellar locomotion. With increasing the Re number of microswimmer, the performance of helical propulsion will relatively reduce. Therefore, larger microorganisms use cilia to provide propulsion [39]. Speed and efficiency of artificial microswimmers, besides ease of fabrication and actuation methods, are enough criteria for functional predominance. Energy generation shortage and battery limitations at microscale necessitate the use of highly efficient microrobots. Even for nonautonomous microdevices, the energy consumption is critical.

Behkam and Sitti [7] have reported efficiency of less than 12% for planar and helical wave propulsion methodologies. They have concluded that having a fully efficient actuator, the planar wave flagellar propulsion has a higher efficiency and provides a higher speed. Abbott et al. [13] considered the effect of magnetic actuation limitations on the microrobot efficiency. They inferred that helical and planar

wave propulsion efficiencies are comparable and higher than gradient magnetic pulling, with considering the magnetic actuation performance. They suggested helical flagellar motion as the most efficient propulsion method. However, they did not report the amounts of efficiency. As calculated in this paper, the *ParaLiker* can achieve a maximum speed between 3–4.5 mm/s. Assuming a 100% efficiency for the actuators, the microrobot possesses a propulsive efficiency of about 21% for 40 numbers of cilia. This value reaches to near 40% for 500 cilia. Although for a rightful and real comparison, the overall efficiency should be computed with taking into account the actuator efficiency, however, the ciliary microrobotic propulsion has a much higher efficiency than flagellar one has.

6.4 High Reynolds Number Microswimmer

Nature uses drag-based swimming for low Re numbers, where sizes are small and motion is slow. Once Re is larger, bigger and faster animals generally swim using inertia-based methods. The inertia-based swimming methodology results in higher speeds and efficiencies. Inertia-based swimming efficiency sometimes exceeds 80%, as we see in pinnipeds and cetaceans [38]. While drag-based propulsion has much lower efficiencies. However, even at high Re numbers, animals rely on drag forces to accelerate from the rest. Therefore, drag-based swimming is an effective propulsion methodology depending on the ecological context in which an animal lives. For instance, muskrat swims paddling its feet and using its tail function [40].

Locomotion in human body blood stream may involve high Re flows, where the flagellar propulsion performance begins to decay [25, 38]. Drag-based swimming using artificial cilia can operate in high Re numbers. As stated, Stokes equation ignores the effect of inertial forces. However, when Re increases, the inertia contributes to microrobot propulsion and results in a higher maximum speed and efficiency. Locomotory capability in turbulent flows enables the proposed microrobot to be entered into the human body through blood stream to carry out its mission. Although many issues may now enfold this idea, however, it is an important target for microrobotics in biomedical applications.

7 Conclusion

Several swimming microrobots inspiring flagellar propulsion methodology can be found in literature. Here, the authors have proposed *ParaLiker*, a novel swimming microrobot based on ciliary motion. Hydrodynamics of artificial cilia was modeled using RFT concept, which relates drag forces to velocities for a viscous regime. Dynamic model of the system was developed to estimate the propulsive force and velocity of the microrobot. Two engines were used in the dynamic model for actuation of artificial cilia, one based on natural cilia and one simple actuation force. Efficiency of the propulsion system was computed and the dependence of microrobot performance on its design parameters was studied.

ParaLiker can swim with a maximum speed between 3–4.5 mm/s. The calculated efficiency reaches to a reasonable value of 40% for a microrobot driven with 500 cilia. Increment of cilia length and diameter increases the propulsive force and velocity of the microrobot. Maximum efficiency can be obtained with a cilia length of 17 μm

and cilia diameter of 24 nm. Increase in cilia numbers drastically increases efficiency of the microrobot. It was shown that, even with a simple actuation engine, the microrobot has a net movement. It has been demonstrated that ciliary motion is a promising methodology for microrobotic swimming, possessing a high thrust, speed and efficiency.

The main challenge in developing *ParaLiker* is actuation of artificial cilia. Many methods have been developed for fabrication and actuation of artificial cilia. However, any practical actuation method should guarantee the asymmetric cilia beating. Cilia unbending during recovery stroke drastically decrease the efficiency of the microrobot.

References

1. Nelson, B.J., Kaliakatsos, I.K., Abbott, J.J.: Microrobots for minimally invasive medicine. Annu. Rev. Biomed. Eng. **12**, 55–85 (2010)
2. Guo, S., Hasegaw, Y., Fukuda, T., Asaka, K.: Fish-like underwater microrobot with multi DOF. In: Proceeding of 2001 IEEE International Symposium on Micromechatronics and Human Science, Nagoya, Japan, pp. 63–68 (2001)
3. Jung, J., Kim, B., Tak, Y., Park, J.: Undulatory tadpole robot (TadRob) using ionic polymer metal composite (IMPC) actuator. In: Proceedings of 2003 IEEE International Conference on Intelligent Robots and Systems, Las Vegas, Nevada, pp. 2133–2138 (2003)
4. Mei, T., Chen, Y., Fu, G., Kong, D.: Wireless drive and control of a swimming microrobot. In: Proceedings of 2002 IEEE International Conference on Robotics & Automation, Washington, DC, pp. 1131–1136 (2002)
5. Zhang, Y., Wang, Q., Zhang, P., Wang, X., Mei, T.: Dynamic analysis and experiment of a 3 mm swimming microrobot. In: Proceedings of 2004 IEEE International Conference on Intelligent Robots and Systems, Sendai, Japan, pp. 1746–1750 (2004)
6. Uchiyama, T., Kikuyama, K.: Numerical simulation for the propulsive performance of a submerged wiggling micromachine. J. Micromech. Microeng. **14**, 1537–1543 (2004)
7. Behkam, B., Sitti, M.: Design methodology for biomimetic propulsion of miniature swimming robot. Trans. ASME J. Dyn. Sys. Meas. Control **128**, 36–43 (2006)
8. Kosa, G., Shoham, M.: Propulsion method for swimming microrobots. IEEE Trans. Rob. **23**, 137–150 (2007)
9. Li, H., Tan, J., Zhang, M.: Dynamics modeling and analysis of a swimming microrobot for controlled drug delivery. In: Proceedings of 2006 IEEE International Conference on Robotics and Automation, Orlando, Florida, pp. 1768–1773 (2006)
10. Yesin, K.B., Vollmers, K., Nelson, B.J.: Modeling and control of untethered biomicrorobots in a fluidic environment using electromagnetic fields. Int. J. Rob. Res. **25**, 527–536 (2006)
11. Guo, S., Pan, Q., Khamesee, M.B.: Development of a novel type of microrobot for biomedical application. Microsyst. Technol. **14**, 307–314 (2008)
12. Zhang, L., Abbott, J.J., Dong, L.X., Kratochvil, B.E., Bell, D., Nelson, B.J.: Artificial bacterial flagella: fabrication and magnetic control. Appl. Phys. Lett. **94**, 064107-064107-3 (2009)
13. Abbott, J.J., Peyer, K.E., Lagomarsino, M.C., Zhang, L., Dong, L., Kaliakatsos, J.K., Nelson, B.J.: How should microrobots swim? Int. J. Rob. Res. **28**, 1434–1447 (2009)
14. Zhang, L., Abbott, J.J., Dong, L., Kathrin, P.E., Kratochvil, B.E., Zhang, H., Bergeles, C., Nelson, B.J.: Characterizing the swimming properties of artificial bacterial flagella. Nano Lett. **9**, 3663–3667 (2009)
15. Kosa, G., Jakab, P., Hata, N., Jolesz, F., Neubach, Z., Shoham, M., Zaaroor, M., Szekely, G.: Flagellar swimming for medical micro robots: theory, experiments and application. In: Proceedings of the 2nd Biennial IEEE/RAS-EMBS International Conference on Biomedical Robotics and Biomechatronics, Scottsdale, AZ, USA, pp. 258–263 (2008)
16. Fountain, T.W.R., Kailat, P.V., Abbott, J.J.: Wireless control of magnetic helical microrobots using a rotating-permanent-magnet manipulator. In: IEEE Int. Conf. Robotics and Automation, pp. 576–581 (2010)

17. Pan, Q., Guo, S., Okada, T.: Development of a wireless hybrid microrobot for biomedical applications. In: Proceedings of the 2010 IEEE/RSJ International Conference on Intelligent Robots and Systems, Taipei, Taiwan, pp. 5768–5773 (2010)
18. Dreyfus, R., Baudry, J., Roper, M.L., Fermigier, M., Stone, H.A., Bibette, J.: Microscopic artificial swimmers. Nature **437**, 862–865 (2005)
19. Martel, S., Mohammadi, M., Felfoul, O., Lu, Z., Pouponneau, P.: Flagellated magnetotactic bacteria as controlled MRI-trackable propulsion and steering systems for medical nanorobots operating in the human microvasculature. Int. J. Rob. Res. **28**, 571–582 (2009)
20. Behkam, B., Sitti, M.: Bacterial flagella-based propulsion and on/off motion control of microscale objects. Appl. Phys. Lett. **90**, 023902-023902-3 (2007)
21. McGary, P.D., Tan, L., Zou, J., Stadler, B.J.H., Downey, P.R., Flatau, A.B.: Magnetic nanowires for acoustic sensors (invited). J. Appl. Phys. **99**, 08B310-08B310-6 (2006)
22. Khaderi, S.N., Baltussen, M.G.H.M., Anderson, P.D., Ioan, D., den Toonder, J.M.J., Onck, P.R.: Nature-inspired microfluidic propulsion using magnetic actuation. Phys. Rev. E **79**, 046304-046304-4 (2009)
23. Liu, C.: Micromachined biomimetic artificial haircell sensors. Bioinspir. Biomim. **2**, S162–S169 (2007)
24. Zhou, Z., Liu, Z.: Biomimetic cilia based on MEMS technology. J. Bionic Eng. **5**, 358–365 (2008)
25. Childress, S.: Mechanics of Swimming and Flying. Cambridge University Press, New York (1981)
26. Taylor, G.I.: Analysis of the swimming of microscopic organisms. Proc. R. Soc. Lond. **A209**, 447–461 (1951)
27. Gray, J., Hancock, G.: The propulsion of sea-urchin spermatozoa. J. Exp. Biol. **32**, 802–814 (1955)
28. Brokaw, C.J.: Bending moments in free-swimming flagella. J. Exp. Biol. **53**, 445–464 (1970)
29. Brennen, C., Winet, H.: Fluid mechanics of propulsion by cilia and flagella. Annu. Rev. Fluid Mech. **9**, 339–398 (1977)
30. Johnson, R.E., Brokaw, C.J.: Flagellar hydrodynamics: a comparison between resistive-force theory and slender-body theory. Biophys. J. **25**, 113–127 (1979)
31. Hines, M., Blum, J.J.: Bend propagation in flagella. I Derivation equations motion simulation. Biophys. J. **23**, 267–340 (1978)
32. Gueron, S., Levit-Gurevich, K.: Computation of the internal forces in cilia: application to ciliary motion, the effects of viscosity, and cilia interactions. Biophys. J. **74**, 1658–1676 (1998)
33. Feng, J., Joseph, D.D., Glowinski, R., Pan, T.W.: A three-dimensional computation of the force and torque on an ellipsoid settling slowly through a viscoelastic fluid. J. Fluid Mech. **283**, 1–16 (1995)
34. Baba, S.A.: Flexural rigidity and elastic constant of cilia. J. Exp. Biol. **56**, 459–467 (1972)
35. Gueron, S., Levit-Gurevich, K.: Energetic considerations of ciliary beating and the advantage of metachronal coordination. Proc. Natl. Acad. Sci. Appl. Math. **96**, 12240–12245 (1999)
36. Khatavkar, V.V., Anderson, P.D., den Toonder, J.M.J., Meijer, H.E.H.: Active micromixer based on artificial cilia. Phys Fluids **19**, 083605-083605-13 (2007)
37. Tabata, O., Kojima, H., Kasatani, T., Isono, Y., Yoshida, R.: Chemo-mechanical actuator using self-oscillating gel for artificial cilia. In: The 16th IEEE International Conference on Micro Electro Mechanical Systems (MEMS2003), pp. 12–15 (2003)
38. Vogel, S.: Modes and scaling in aquatic locomotion. Integr. Comp. Biol. **48**, 702–712 (2008)
39. Vogel, S.: Life in Moving Fluids, 2nd edn. Princeton University Press, Princeton (1994)
40. Fish, F.E.: Function of the compressed tail of surface swimming muskrats (Ondatra zibethicus). J. Mammal. **63**, 591–597 (1982)